Published in final edited form as:
ACS Nano. 2007 November 30; 1(4): 258–264. doi:10.1021/nn700062z.

Multi-Modal Nano-Probes for Radionuclide and 5-color Near Infrared Optical Lymphatic Imaging

Hisataka Kobayashi[†,*], **Yoshinori Koyama**[†], **Tristan Barrett**[†], **Yukihiro Hama**[†], **Celeste A. S. Regino**[‡], **In Soo Shin**[§], **Beom-Su Jang**[§], **Nhat Le**[§], **Chang H. Paik**[§], **Peter L. Choyke**[†], and **Yasuteru Urano**[⊥]

† *Molecular Imaging Program, NIH, Bethesda, Maryland 20892-1088, USA*

‡ *Radiation Oncology Branch, Center for CancerResearch, National Cancer Institute, NIH, Bethesda, Maryland 20892-1088, USA*

§ *Nuclear Medicine Department, Warren Magnuson Clinical Center, NIH, Bethesda, Maryland 20892, USA*

⊥ *Graduate School of Pharmaceutical Sciences, The University of Tokyo, 7-3-1 Hongo, Bunkyo-ku, Tokyo 113-0033, Japan*

Abstract

Current contrast agents generally have one function and can only be imaged in monochrome, therefore, the majority of imaging methods can only impart uniparametric information. A single nano-particle has the potential to be loaded with multiple payloads. Such multi-modality probes have the ability to be imaged by more than one imaging technique, which could compensate for the weakness or even combine the advantages of each individual modality. Furthermore, optical imaging using different optical probes enables us to achieve multi-color *in vivo* imaging, wherein multiple parameters can be read from a single image. To allow differentiation of multiple optical signals *in vivo*, each probe should have a close but different near infrared emission. To this end, we synthesized nano-probes with multi-modal and multi-color potential, which employed a polyamidoamine dendrimer platform linked to both radionuclides and optical probes, permitting dual-modality scintigraphic and 5-color near infrared optical lymphatic imaging using a multiple excitation spectrally-resolved fluorescence imaging technique.

Keywords

dendrimer; scintigraphy; near infrared; fluorescence imaging; multiple modalities; multiple colors; lymphatic imaging

No imaging modality is perfect. Each has its own distinct advantages and limitations. The simultaneous use of two or more modalities can help to overcome the limitation of each individual method and increase or improve the information obtained during an examination session. The combined use of Computed Tomography (CT) and Positron Emission Tomography (PET) is a successful example of multi-modal imaging: CT provides high resolution anatomical detail and PET provides functional information [1]. Currently they are very few examples of multi-modal imaging probes that can be detected by more than one technique: dual agents for recognition by both radionuclide and optical imaging [2,3], or Magnetic Resonance (MR) and optical imaging [4–8].

*Corresponding author: Hisataka Kobayashi, MD, PhD, Molecular Imaging Program, Cancer for Cancer Research, NCI/NIH, Bldg. 10, Room 1B40, MSC 1088, Bethesda, Maryland 20892-1088, USA, E-mail: Kobayash@mail.nih.gov.

Furthermore, the conventional imaging methods are generally monochrome and only able to detect one contrast agent at a time, limiting us to single parametric data. Single photon scintigraphy has been shown to have potential for simultaneously detecting two different imaging agents, *i.e.* technetium-99m and thallium-201, by energy resolution [9]. However, in this case, both the spatial and the energy resolutions were poor and did not allow for the reconstruction of a precise image from each agent. Multi-color optical imaging is simple to achieve with the technique of spectrally resolved imaging. Herein, two or more optical agents can be differentiated on the basis of their different emission spectra. Multi-color imaging is already commonplace in microscopic imaging and is beginning to be utilized for *in vivo* imaging [10–12]. However, *in vivo* imaging is essentially limited to long wavelength dyes that emit in the near-infrared (NIR) range (650–850 nm), in order to maximize depth penetration and limit the autofluorescence, background signal [13].

With this in mind we have synthesized multi-modal, multi-color nano-sized imaging probes with nearly identical chemical characteristics. This single injection imaging probe offers the potential for both multi-modal imaging and multi-color resolution.

RESULTS AND DISCUSSION

Using a generation-6 PAMAM dendrimer with an ethylenediamine core as the platform component, ^{111}In-labeled radionuclide/5-colored NIR optical dual-modal imaging probes were successfully synthesized with multiple steps as shown in Figure 1. The final products contained 120 SCN-Bz-DTPA molecules and 4 NIR dyes covalently conjugated with the terminal amino groups. All probes were of ~8 nm in diameter as determined by both dynamic light scattering (DLS): 8.1±0.1 nm, and gel-filtration: 8.5 nm (Figure 2). Both radionuclide imaging and 5-color NIR spectral fluorescence imaging were able to show the lymphatic drainage patterns in the head and neck regions of the mice examined (Figure 3a). Visualization of lymphatic drainage was consistently seen even after shuffling the pattern of injection sites (Figure 3c). All draining lymph nodes (LNs) were subsequently validated by both *ex vivo* radionuclide and 5-color NIR spectral fluorescence imaging of the resected LNs, and were confirmed to represent LNs on cut section (Figure 3b, 3d). The radionuclide imaging provided semi-quantitative information in addition to the qualitative 5-color NIR optical imaging both *in vivo* and *ex vivo* that re-evaluated the variation of lymphatic drainage even in mice of the same strain [11,14].

The design of the final product, **c: G6-(Bz-DTPA)$_{119}$-(NIR)$_4$-(Bz-DTPA-111In)$_1$** was rationally designed based on the need to develop a successful and easy-to-use dual-modal multicolor lymph node imaging agent. Bz-DTPA molecules were conjugated to more than half of the available surface amine residues on a dendrimer molecule for the following three reasons; 1. suppressing the poly-cation toxicity of dendrimer by changing the charge [15], 2. facilitating efficient and stable ^{111}In-labeling to eventually enable this agent to be produced in a kit form by adding sufficient number of chelate molecules, 3. leaving open the possibility to conjugate another metal for additional imaging applications (e.g. Gd ions for MRI contrast) [8,16], 4. retaining terminal amino groups for the conjugating to targeting ligands [17]. The kit form for labeling the dendrimer with ^{111}In requires no purification with gel-filtration after mixing with ^{111}In acetate and thus, facilitates the use in clinical practice. In reality, ITLC data showed that more than 96.9% of ^{111}In was associated with final product c in all 5 compounds before purification indicating high coefficients of binding (Supporting fugure 1a). The additional purification step using G-50 columns did not show any advantages over pre-purified compounds (Supporting figure 1b). Therefore, as we intended, intermediate product b could be radiolabeled with ^{111}In acetate just by mixing and this enables the use of b as a pre-labeling kit form.

Four NIR dye molecules were conjugated with a single molecule of intermediate product **a**. Since the quantum yield of each NIR dye molecule generally decreased when more than 2 dyes were conjugated with a G6 dendrimer-DTPA conjugate [8], quantum yield of a conjugate did not proportionally increase as the number of conjugated dyes increased. In addition, if too many dyes were placed on a single G6 conjugate, dyes quenched [8,18]. Therefore, 4 NIR dye molecules on each dendrimer conjugate were proved to be the optimal design.

Local lymphatic drainage is an important route for the metastasis of cancer cells. To this end, identification of the sentinel lymph node and its biopsy has recently become a common staging procedure for cancers which frequently metastasize to the local lymph nodes, *i.e.* breast cancer [19,20], and malignant melanoma [21,22]. However, access to the lymphatic vessels is difficult [23]. Unlike the blood circulation, the lymphatics are one-way, single circulatory systems, from peripheral to central. Furthermore, the lymphatic vessels are complicated small structures, making direct cannulation difficult [24]. Thus indirect uptake following interstitial injection of an agent is preferable, although it brings with it greater concerns regarding the pharmacokinetics of their lymphatic drainage. In order to visualize the local lymphatic drainage and detect sentinel lymph nodes (SLNs), the two most commonly used methods employ peritumoral injections of either a radionuclide labeled sulfur or albumin colloid, or isosulfan blue dye [25]. Radionuclide imaging has the advantage of increased depth detection, but is limited in its spatial resolution [26]. The dye method requires dissection of tissue until the "dyed" SLN is visually detected. In addition, staining of the blue dye at the injection site may present a potent cosmetic problem for breast cancer patients, who subsequently receive breast-conserving surgery. NIR optical imaging offers a means to overcome some of these limitations because they are colorless and can be detected through tissue for 1–2cm. Indeed, NIR fluorescent quantum dots (Qdots) have been employed successfully *in vivo* imaging of the lymphatics in order to detect the SLN arising from breast tissue [27].

However, optical imaging using Qdots is still limited in its depth penetration, and by the potential toxicity of the probes, which contain heavy metals, *e.g.* cadmium and selenium in Qdots [28,29]. In addition, in order to make multicolor Qdots each Qdot must be a slightly different size (~2 nm), which might lead to changes in the kinetics of their lymphatic drainage especially from the subcutaneous tissue such as the breast, where the lymphatic drainage is not as active as in the intradermal tissue [11]. In order to overcome the limitation of depth, we have recently reported an MRI and NIR optical dual-modal dendrimer-based probe for SLN detection. However, the low sensitivity of MRI for Gadolinium contained upon the dendrimer structure necessitates a relatively large dose of the agent [8] and MRI is relatively impractical for imaging prior to surgery.

In order to minimize these problems, we have developed a series of dual-modal imaging probes with similar chemical and physical characteristics containing both radionuclide and multi-color organic NIR fluorophores based on a dendrimer platform. Radionuclide imaging of this dual-modal imaging probe allows increased depth penetration and absolute quantification whereas multi-color NIR optical imaging offers excellent real time spatial resolution and the ability to distinguish multiple lymphatic drainages. Both of these methods have a matched high sensitivity that allows for a minimization of the required injection dose.

Using Qdots it is possible to obtain 5 separate emission lights within the NIR range from 5 distinct organic NIR dyes with sufficient signal strength, using a single excitation light. Unfortunately, Qdots are unlikely to be used in humans as currently constituted. It was difficult to resolve the spectra of the 5 distinct organic NIR dyes using a single excitation light source because of either low excitation/sensitivity for one or more NIR dyes or cross contamination of 2 NIR dyes (Supporting figures 2). Therefore, we employed 3 different excitation filters to differentially excite 5 distinct organic NIR dyes in the 650 nm to 800 nm range (Figure 1). The

use of organic NIR dyes enabled us to conjugate 5 different NIR fluorophores to PAMAM dendrimers with nearly identical size and chemical characteristics. Chelating a radionuclide to the dendrimer was also stably performed because a large number of chelating agents were conjugated on the surface of the dendrimer. Therefore, each injection was performed with a nearly identical construct with similar bright emission light, differing only in the wavelength of the NIR light emitted, so that successful images could be taken even after shuffling the patterns of injection.

In conclusion, multi-modal, multi-color nano-sized imaging probes for radionuclide and NIR fluorescence imaging were successfully synthesized and applied for *in vivo* lymphatic imaging of the head and neck region of mice. Radionuclide imaging provided semi-quantitative information, whilst optical imaging provided qualitative information for each of the 5 lymphatic basins, with excellent spatial resolution. This method may find application in sentinel node imaging of human tumors.

METHODS

Conjugation of the chelating agent to dendrimers

A polyamidoamine dendrimer (PAMAM-G6) [Aldrich Chemical Co., Milwaukee, WI] with an ethylenediamine core, the generation-6 interior (G = 6), maximum 256 terminal primary amino groups, and a molecular weight of 58,048 Dalton was used for the basic platform structure. The schema of the synthetic reaction is shown in Figure 1. PAMAM-G6 solution concentrated to 12 mg (210 nmol) in 2 mL of phosphate buffer at pH 8.5 was reacted with 60 mg (~85 μmol) of the 2-(*p*-isothiocyanatobenzyl)-diethylenetriamine-pentaacetic acid (SCN-Bz-DTPA; ~700Da) [Maclocyclic, Dallas, TX] at 40°C for 48 hrs. The resulting preparation was purified by diafiltration using the Centricon 30 (Amicon Co., Beverly, MA). The number of SCN-Bz-DTPA molecules conjugated per dendrimer was determined by a previously-described ^{111}In -labeling assay [30,31]. Briefly, a 5μL aliquot of the reaction mixture was reacted with ^{111}In chloride in 45 μL of 0.2 M sodium acetate buffer at pH 4.2 for 1 hr at room temperature. The radiolabeled sample was analyzed with size-exclusion HPLC equipped with a TSK G3000SWxL column (Tosoh Bioscience LLC, Montgomeryville, PA; 0.067 M PB-0.1 M KCl, pH 6.8; 1 ml/min) and an online radioactivity detector (Bioscan, Washington, DC). The HPLC profile showed 29% of the total ^{111}In-radioactivity was associated with the PAMAM-G6 fraction. Therefore, 120 SCN-Bz-DTPA molecules were conjugated per one PAMAM-G6 molecule (a: G6-(Bz-DTPA)$_{120}$ in Figure 1;MW: 116kD).

Conjugation of near infrared fluorescent dyes

Amino-reactive Alexa 660, 680, 700, and 750-succinoimidyl ester were purchased from Molecular Probes Inc. (Eugene, OR, USA). Amino-reactive Cy5-succinoimidyl ester was purchased from GE Healthcare Limited (Piscateway, NJ, USA). At room temperature, 2 mg (17 nmol) of (**a: G6-(Bz-DTPA)$_{120}$**) in 400 μL of 0.3M Na_2HPO_4, pH 8.5 was rapidly mixted with 170nmol (34 μL/5 mM) of each of fluorescent dyes-succinoimidyl ester in DMSO, and the reaction mixture was incubated for 15 min. The mixture was purified with Sephadex G50 (PD-10; GE Healthcare, Milwaukee, WI, USA).

The G6-(Bz-DTPA)$_{120}$ concentration of NIR dye-conjugated samples was determined with Coomassie Plus protein assay kit (Pierce Chem Co., Rockford, IL, USA) by measuring the absorption at 595 nm with a UV-Vis spectroscopy (8453 Value UV-Bis system, Agilent Technologies, Palo Alto, CA, USA) using known concentrations of G6-(Bz-DTPA)$_{120}$ (20, 50 and 100 μg/mL) as standard solutions. The concentrations of Cy5, Alexa660, 680, 700, and 750 were measured by their absorption at 651, 665, 681, 703, and 753 nm, respectively, using the UV-Vis system to confirm the number of fluorophore molecules conjugated with each G6

dendrimer molecule. The number of fluorophore molecules per G6-(Bz-DTPA)$_{120}$ was 4.1, 3.9, 3.6, 3.9, and 4.0 for Cy5, Alexa660, 680, 700, and 750, respectively (**b: G6-(Bz-DTPA)$_{120}$-(NIR)$_4$ in** Figure 1). The yields of **b** were 91–93% for G6-(Bz-DTPA)$_{120}$ and 36–41% of NIR dye molecules were conjugated with G6-(Bz-DTPA)$_{120}$

Radiolabeling with ^{111}In

Carrier-free $^{111}InCl_3$ was purchased from PerkinElmer (Wellesley, MA). Dendrimers conjugated with NIR dyes (G6-(Bz-DTPA)$_{120}$-(NIR)$_4$) were reacted with ^{111}In in 0.2 M sodium acetate buffer at pH 4.2 for 1 hr at room temperature, as previously described [32]. DTPA solution at a final concentration of 0.2 mM was added to the radiolabeled products to complex potential free ^{111}In remaining in the product solution. The specific activities of all radiolabeled nano-probes were similar, ranging from 12.1 to 12.3 mCi/mg (**c: G6-(Bz-DTPA)$_{119}$-(NIR)$_4$-(Bz-DTPA-111In)$_1$** in Figure 1). The radiolabeling yield of the radiolabeled nano-probes was >98% as determined by instant thin layer chromatography (ITLC; Gelman Sciences Ann Arbor, MI) developed with a solvent mixture containing 3:2:1 methanol:10% ammonium acetate in water:0.5 M citric acid and size-exclusion HPLC using a TSK G3000PWxL column (Tosoh Bioscience LLC, Montgomeryville, PA; 0.067 M PB-0.1 M KCl, pH 6.8; 1 ml/min). On ITLC, ^{111}In labeled G6 dendrimers remain at the origin, whereas free ^{111}In moves to the solvent front as ^{111}In-DTPA or ^{111}In-acetate. Retention times of all final products detected by an in-line fluorescence detector (FP2020, Jasco Inc., Easton, MD, USA)were 20.7 min on the size-exclusion HPLC using a TSK G6000PW column (Figure 4a–e) and those detected by an in-line NaI gamma detector (γRAM, IN/US Systems, Inc., Fairfield, NJ) were 7.3 min on the size-exclusion HPLC using a TSK G3000PWxL column (Figure 4f). Both fluorescent and radioactive purity of all final compounds **c** were >98% on size-exclusion HPLCs.

Measurement of the physical size of the agents

The physical sizes of all agents were analyzed with gel-filtration using a high-performance liquid chromatography (HPLC) system (System Gold, Beckman Coulter, Inc., Fullerton, CA) equipped with TSK G6000PW 30cm column (Tosoh Bioscience LLC, Montgomeryville, PA) and Shodex KW405-4F, 30 cm column (Showa Denko America, Inc., New York, NY) with 0.066M PBS, and Hydrodynamic light scattering (DLS) using a Malvern Zeta Sizer Nano instrument (Malvern Instruments Ltd., Malvern, UK) with 0.066M PBS. The size calculation with HPLC was performed by using known sided pure protein standards; IgM (22 nm), thyroglobuin (17 nm), IgG (11 nm) and albumin (7 nm). Flow rates were 0.5 ml/min for TSK G6000PW and 0.3 ml/min for Shodex KW405-4F. The absorbance at 280 nm was monitored. DLS was performed using the agent alone before the conjugated NIR dyes (**a: G6-(Bz-DTPA)$_{120}$ in** Figure 1) because NIR fluorescence interfered the light scattering signal of DLS.

In vivo multiple excitation wavelength-resolved 5-color spectral fluorescence and radionuclide imaging

All *in vivo* procedures were carried out in compliance with the Guide for the Care and Use of Laboratory Animal Resources (1996), National Research Council, and approved by the National Cancer Institute Animal Care and Use Committee.

10-week-old normal athymic female mice were anesthetized *via* intraperitoneal injection of 1.5 mg/300μL sodium pentobarbital (Dainabot, Osaka, Japan). The mice were administered intracutaneous injections of 10 μL/10 μCi (350 pmol for NIR dyes) of each G6-(Bz-DTPA)$_{119}$-(NIR)$_4$-(Bz-DTPA-^{111}In)$_1$ conjugate into one of 5 sites: the middle phalange of the left or right upper extremity, the left or right ear, and the median chin. For the first 5 consecutive mice only spectral fluorescence imaging was performed.

The next 5 mice only underwent radionuclide imaging. Injection points were rotated in each mouse (as shown in Table 1) in order to validate that changing the injection pattern did not affect the imaging quality. Subsequently, another 3 consecutive mice received both spectral fluorescence and radionuclide imaging to allow for direct comparison of the imaging techniques.

For spectral fluorescence imaging, within 10 min after injection of the agent, when both lymphatic ducts and lymph nodes could be shown clearly [11,33], wavelength-resolved spectral imaging was carried out using a spectral imaging system (Maestro In-Vivo Imaging System, CRi Inc., Woburn, MA, USA). Animals were placed in the spinal position whilst under pentobarbital anesthesia. The injection sites were masked with a non-fluorescent black tape because the signal from the injection site would otherwise overwhelm the dynamic range of the camera, rendering the un-mixing algorithm non-functional. After obtaining *in vivo* images, lymphadenectomy was performed and another spectral fluorescence image was obtained during surgery. All of the removed LNs were validated by *ex vivo* spectral fluorescence imaging. Three excitation band pass and emission long pass filters of 575–605/645, 615–665/700 and 671–705/750 nm (excitation/emission) were consecutively used. The tunable filter was automatically stepped in 5-nm increments from 630 to 850, from 680 to 950, and from 730 to 950 nm for 575–605/645, 615–665/700 and 671–705/750 nm filter sets, respectively, using the same exposure time for images captured at each wavelength (Figure 1). Each acquisition with this 3-excitation spectral fluorescence imaging technique took approximately 2 minutes. Collected images were analyzed by the Maestro software (Nuance Ver 2.22, CRi), which uses multi-spectral un-mixing algorithms to separate autofluorescence from NIR dye signals, and a composite image consisting of all 5 NIR dye signals and autofluorescence was generated using a spectral library obtained from each lymph node injected either with one of G6-(Bz-DTPA)$_{119}$-(NIR)$_4$-(Bz-DTPA-^{111}In) solutions.

For radionuclide imaging, within 10 min after injection of the agent, radionuclide imaging was carried out using an imaging plate (BAS-SR 2025, Fujifilm Medical Systems USA, Inc., Stamford, CT). Animals were placed in the supine position on the imaging plate immediately after sacrifice by over-dose intravenous injection of pentobarbital. The injection sites of the skin were removed as much as possible because the signal from the injection site would otherwise overwhelm the dynamic range of the imaging plate and contaminate the adjacent background. After obtaining postmortem *in situ* images by 10 min exposure, images were developed with 50 μm resolution using a high resolution imaging system (FLA-5100, Fujifilm Medical Systems USA). After obtaining *in vivo* images, lymphadenectomy was performed. All removed LNs were validated using *ex vivo* radionuclide imaging as described above.

For the comparison experiments, *in vivo* multi-excitation spectral fluorescence imaging was performed within 10 min of injection, followed by postmortem *in situ* radionuclide imaging. Spectral fluorescence imaging of *ex vivo* lymph nodes was then carried out, followed by the radionuclide imaging.

Supplementary Material

Refer to Web version on PubMed Central for supplementary material.

Acknowledgements

This research was supported by the Intramural Research Program of the NIH, National Cancer Institute, Center for Cancer Research.

REFERENCES AND NOTES

1. Blodgett TM, Meltzer CC, Townsend DW. Pet/Ct: Form and Function. Radiology 2007;242:360–385. [PubMed: 17255408]
2. Bullok KE, Dyszlewski M, Prior JL, Pica CM, Sharma V, Piwnica-Worms D. Characterization of Novel Histidine-Tagged Tat-Peptide Complexes Dual-Labeled with (99m)Tc-Tricarbonyl and Fluorescein for Scintigraphy and Fluorescence Microscopy. Bioconjug Chem 2002;13:1226–1237. [PubMed: 12440857]
3. Houston JP, Ke S, Wang W, Li C, Sevick-Muraca EM. Quality Analysis of *In Vivo* Near-Infrared Fluorescence and Conventional Gamma Images Acquired Using a Dual-Labeled Tumor-Targeting Probe. J Biomed Opt 2005;10:054010. [PubMed: 16292970]
4. Huber MM, Staubli AB, Kustedjo K, Gray MH, Shih J, Fraser SE, Jacobs RE, Meade TJ. Fluorescently Detectable Magnetic Resonance Imaging Agents. Bioconjug Chem 1998;9:242–249. [PubMed: 9548540]
5. Josephson L, Kircher MF, Mahmood U, Tang Y, Weissleder R. Near-Infrared Fluorescent Nanoparticles as Combined MR/Optical Imaging Probes. Bioconjug Chem 2002;13:554–560. [PubMed: 12009946]
6. Kircher MF, Mahmood U, King RS, Weissleder R, Josephson L. A Multimodal Nanoparticle for Preoperative Magnetic Resonance Imaging and Intraoperative Optical Brain Tumor Delineation. Cancer Res 2003;63:8122–8125. [PubMed: 14678964]
7. Dafni H, Cohen B, Ziv K, Israely T, Goldshmidt O, Nevo N, Harmelin A, Vlodavsky I, Neeman M. The Role of Heparanase in Lymph Node Metastatic Dissemination: Dynamic Contrast-Enhanced MRI of EB Lymphoma in Mice. Neoplasia 2005;7:224–233. [PubMed: 15799822]
8. Talanov VS, Regino CA, Kobayashi H, Bernardo M, Choyke PL, Brechbiel MW. Dendrimer-Based Nanoprobe for Dual Modality Magnetic Resonance and Fluorescence Imaging. Nano Lett 2006;6:1459–1463. [PubMed: 16834429]
9. Foster GS, Bekerman C, Blend MJ, Byrom E, Pinsky SM. Preoperative Imaging in Primary Hyperparathyroidism. Role of Thallium-Technetium Subtraction Scintigraphy. Arch Otolaryngol Head Neck Surg 1989;115:1197–1202. [PubMed: 2551344]
10. Hoffman RM. The Multiple Uses of Fluorescent Proteins to Visualize Cancer. In Vivo Nat Rev Cancer 2005;5:796–806.
11. Hama Y, Koyama Y, Urano Y, Choyke PL, Kobayashi H. Simultaneous Two-Color Spectral Fluorescence Lymphangiography with Near Infrared Quantum Dots to Map Two Lymphatic Flows from the Breast and the Upper Extremity. Breast Cancer Res Treat 2007;103:23–28. [PubMed: 17028977]
12. Kobayashi H, Hama Y, Koyama Y, Barrett T, Regino CA, Urano Y, Choyke PL. Simultaneous Multicolor Imaging of Five Different Lymphatic Basins Using Quantum Dots. Nano Lett 2007;7:1711–1716. [PubMed: 17530812]
13. Mahmood U. Near Infrared Optical Applications in Molecular Imaging. Earlier, More Accurate Assessment of Disease Presence, Disease Course, and Efficacy of Disease Treatment. IEEE Eng Med Biol Mag 2004;23:58–66. [PubMed: 15508386]
14. Kobayashi H, Kawamoto S, Sakai Y, Choyke PL, Star RA, Brechbiel MW, Sato N, Tagaya Y, Morris JC, Waldmann TA. Lymphatic Drainage Imaging of Breast Cancer in Mice by Micro-Magnetic Resonance Lymphangiography Using a Nano-Size Paramagnetic Contrast Agent. J Natl Cancer Inst 2004;96:703–708. [PubMed: 15126607]
15. Kobayashi H, Sato N, Kawamoto S, Saga T, Hiraga A, Ishimori T, Konishi J, Togashi K, Brechbiel MW. 3D MR Angiography of Intratumoral Vasculature Using a Novel Macromolecular MR Contrast Agent. Magn Reson Med 2001;46:579–585. [PubMed: 11550252]
16. Kobayashi H, Brechbiel MW. Nano-Sized MRI Contrast Agents with Dendrimer Cores. Adv Drug Deliv Rev 2005;57:2271–2286. [PubMed: 16290152]
17. Wiener EC, Konda S, Shadron A, Brechbiel M, Gansow O. Targeting Dendrimer-Chelates to Tumors and Tumor Cells Expressing the High-Affinity Folate Receptor. Invest Radiol 1997;32:748–754. [PubMed: 9406015]

18. Weissleder R, Tung CH, Mahmood U, Bogdanov A Jr. *In Vivo* Imaging of Tumors with Protease-Activated near-Infrared Fluorescent Probes. Nat Biotechnol 1999;17:375–378. [PubMed: 10207887]
19. Chao C, McMasters KM. Sentinel Lymph Node Biopsy in Breast Cancer. Methods Mol Med 2006;120:91–111. [PubMed: 16491597]
20. Ferrari A, Rovera F, Dionigi P, Limonta G, Marelli M, Besana Ciani I, Bianchi V, Vanoli C, Dionigi R. Sentinel Lymph Node Biopsy as the New Standard of Care in the Surgical Treatment for Breast Cancer. Expert Rev Anticancer Ther 2006;6:1503–1515. [PubMed: 17069533]
21. Essner R. Sentinel Lymph Node Biopsy and Melanoma Biology. Clin Cancer Res 2006;12:2320s–2325s. [PubMed: 16609052]
22. Uren RF. Sentinel Lymph Node Biopsy in Melanoma. J Nucl Med 2006;47:191–195. [PubMed: 16455622]
23. Moskovic E, Fernando I, Blake P, Parsons C. Lymphography--Current Role in Oncology. Br J Radiol 1991;64:422–427. [PubMed: 2036566]
24. Davis MJ. An Improved, Computer-Based Method to Automatically Track Internal and External Diameter of Isolated Microvessels. Microcirculation 2005;12:361–372. [PubMed: 16020082]
25. Kim T, Giuliano AE, Lyman GH. Lymphatic Mapping and Sentinel Lymph Node Biopsy in Early-Stage Breast Carcinoma: A Metaanalysis. Cancer 2006;106:4–16. [PubMed: 16329134]
26. Alazraki NP, Styblo T, Grant SF, Cohen C, Larsen T, Aarsvold JN. Sentinel Node Staging of Early Breast Cancer Using Lymphoscintigraphy and the Intraoperative Gamma-Detecting Probe. Semin Nucl Med 2000;30:56–64. [PubMed: 10656244]
27. Kim S, Lim YT, Soltesz EG, De Grand AM, Lee J, Nakayama A, Parker JA, Mihaljevic T, Laurence RG, Dor DM, Cohn LH, Bawendi MG, Frangioni JV. Near-Infrared Fluorescent Type II Quantum Dots for Sentinel Lymph Node Mapping. Nat Biotechnol 2004;22:93–97. [PubMed: 14661026]
28. Hardman R. A Toxicologic Review of Quantum Dots: Toxicity Depends on Physicochemical and Environmental Factors. Environ Health Perspect 2006;114:165–172. [PubMed: 16451849]
29. Cho SJ, Maysinger D, Jain M, Roder B, Hackbarth S, Winnik FM. Long-Term Exposure to CdTe Quantum Dots Causes Functional Impairments in Live Cells. Langmuir 2007;23:1974–1980. [PubMed: 17279683]
30. Kobayashi H, Sato N, Hiraga A, Saga T, Nakamoto Y, Ueda H, Konishi J, Togashi K, Brechbiel MW. 3D-Micro-MR Angiography of Mice Using Macromolecular MR Contrast Agents with Polyamidoamine Dendrimer Core with References to Their Pharmacokinetic Properties. Magn Reson Med 2001;45:454–460. [PubMed: 11241704]
31. Kobayashi H, Sakahara H, Hosono M, Shirato M, Kondo S, Miyatake S, Kikuchi H, Namba Y, Endo K, Konishi J. Scintigraphic Detection of Neural-Cell-Derived Small-Cell Lung Cancer Using Glioma-Specific Antibody. J Cancer Res Clin Oncol 1994;120:259–262. [PubMed: 8126056]
32. Kobayashi H, Wu C, Yoo TM, Sun BF, Drumm D, Pastan I, Paik CH, Gansow OA, Carrasquillo JA, Brechbiel MW. Evaluation of the in Vivo Biodistribution of Yttrium-Labeled Isomers of CHX-DTPA-Conjugated Monoclonal Antibodies. J Nucl Med 1998;39:829–836. [PubMed: 9591585]
33. Kobayashi H, Kawamoto S, Star RA, Waldmann TA, Tagaya Y, Brechbiel MW. Micro-Magnetic Resonance Lymphangiography in Mice Using a Novel Dendrimer-Based Magnetic Resonance Imaging Contrast Agent. Cancer Res 2003;63:271–276. [PubMed: 12543772]

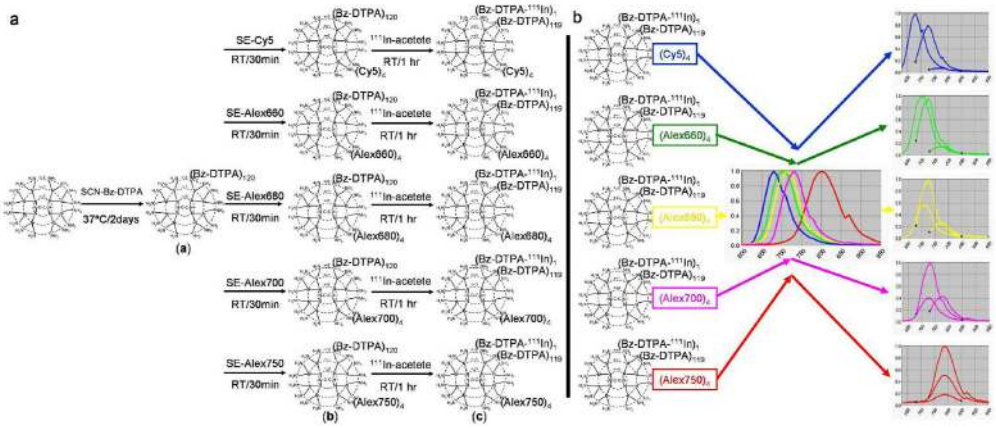

Figure 1. Schema of the synthesis method and the spectral library of nano-probes

The brief synthesis method and single and multiple emission spectra of each nano-probe are schematically shown. As for multiple emission spectra, curve 1, 2, and 3 in each spectra were obtained with three different combined excitation/emission filter settings, respectively, for 575–605 nm/630–850 nm, 615–665 nm/680–950 nm, and 671–705 nm/730–950 nm, respectively.

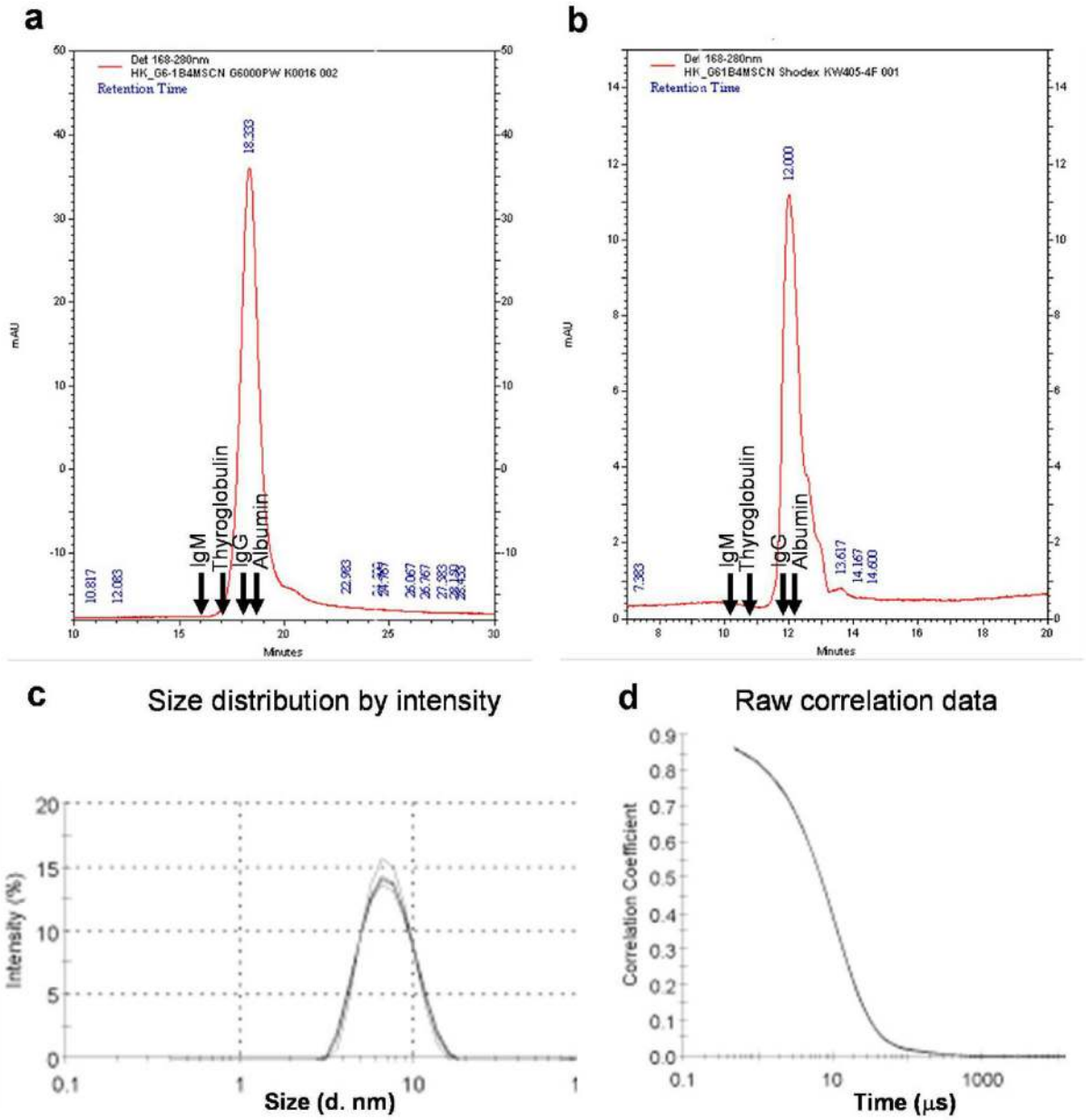

Figure 2. Size measurements

HPLC traces of G6-(Bz-DTPA)$_{120}$ using TSK G6000PW (**a**) and Shodex KW405-4F (**b**) are shown. Standard proteins: IgM (24 nm); 16.08 and 10.10 min, thyroglobulin; (17 nm); 17.12 and 10.78 min, IgG (11 nm); 18.17 and 11.85 min, and Bovine albumin (7 nm) 18.42 and 12.09 min. The calculated diameter with gel-filtration using both columns was 8.5 nm. DLS traces of 5 runs for G6-(Bz-DTPA)$_{120}$ were identical for both distribution of molecular size **(c)** and correlation coefficient (**d**). Two other probes (G6-(Bz-DTPA)$_{123}$ and G6-(Bz-DTPA)$_{113}$), which were not used for the synthesis of the final product, demonstrated identical DLS traces (n=5) and size distributions in each samples as shown in (**c**) and (**d**). The calculated diameter with DLS was 8.1±0.1 nm.

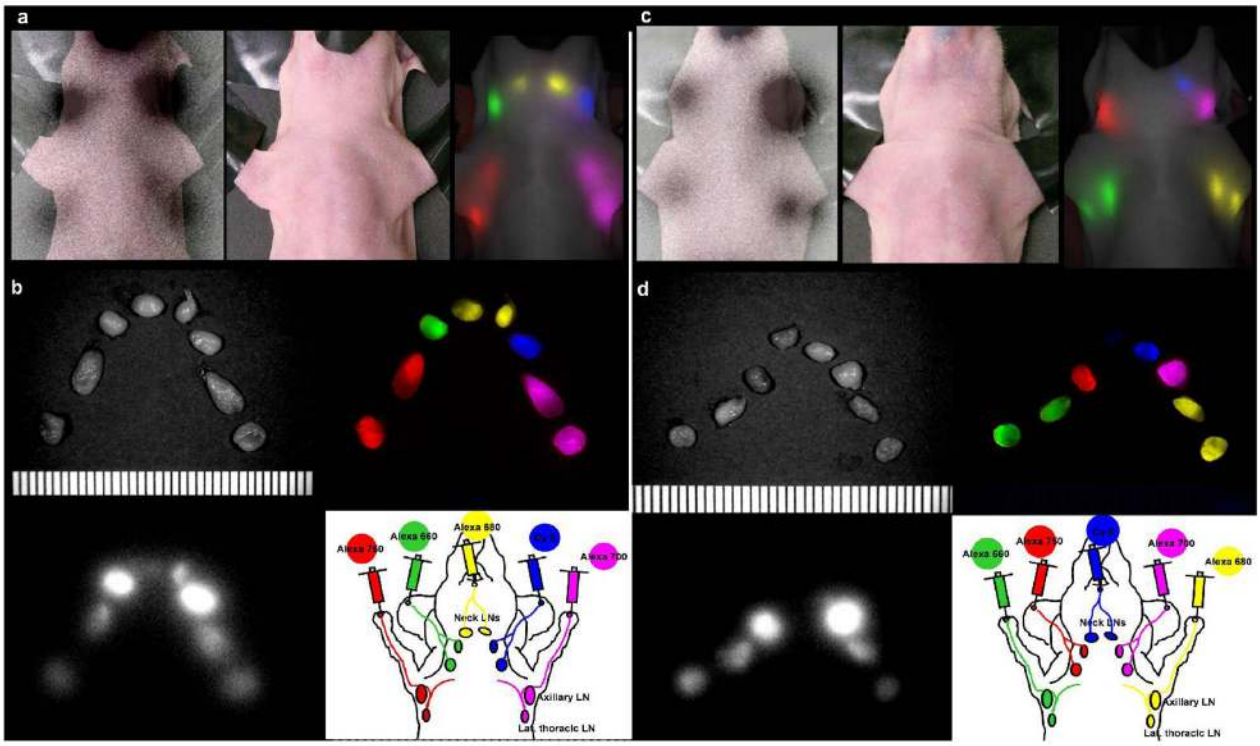

Figure 3. ***In vivo*** **dual-modal, 5-color lymphatic drainage imaging with the ability to visualize 5 distinct lymphatic drainages**

(**a**) *In vivo* multi-excitation spectral fluorescence (right) and postmortem *in situ* radionuclide (left) images of a mouse injected with 5 distinct G6-(Bz-DTPA)$_{119}$-(NIR)$_4$-(Bz-DTPA-^{111}In)$_1$ nanoprobes intracutaneously into the middle digits of the bilateral upper extremities, the bilateral ears, and at the median chin, as shown in the schema (mouse #7 in Table 1). Five primary draining lymph nodes were simultaneously visualized with different colors through the skin in the *in vivo* spectral fluorescence image and are more quantitatively seen in the radionuclide image. (**b**) *Ex vivo* spectral fluorescence and radionuclide images of resected 8 draining lymph nodes correlate well to the *in vivo* imaging. Images of a different mouse (mouse #8 in Table 1), given shuffled injections, are shown in (**c**) and (**d**). The imaging results were consistent for all mice examined.

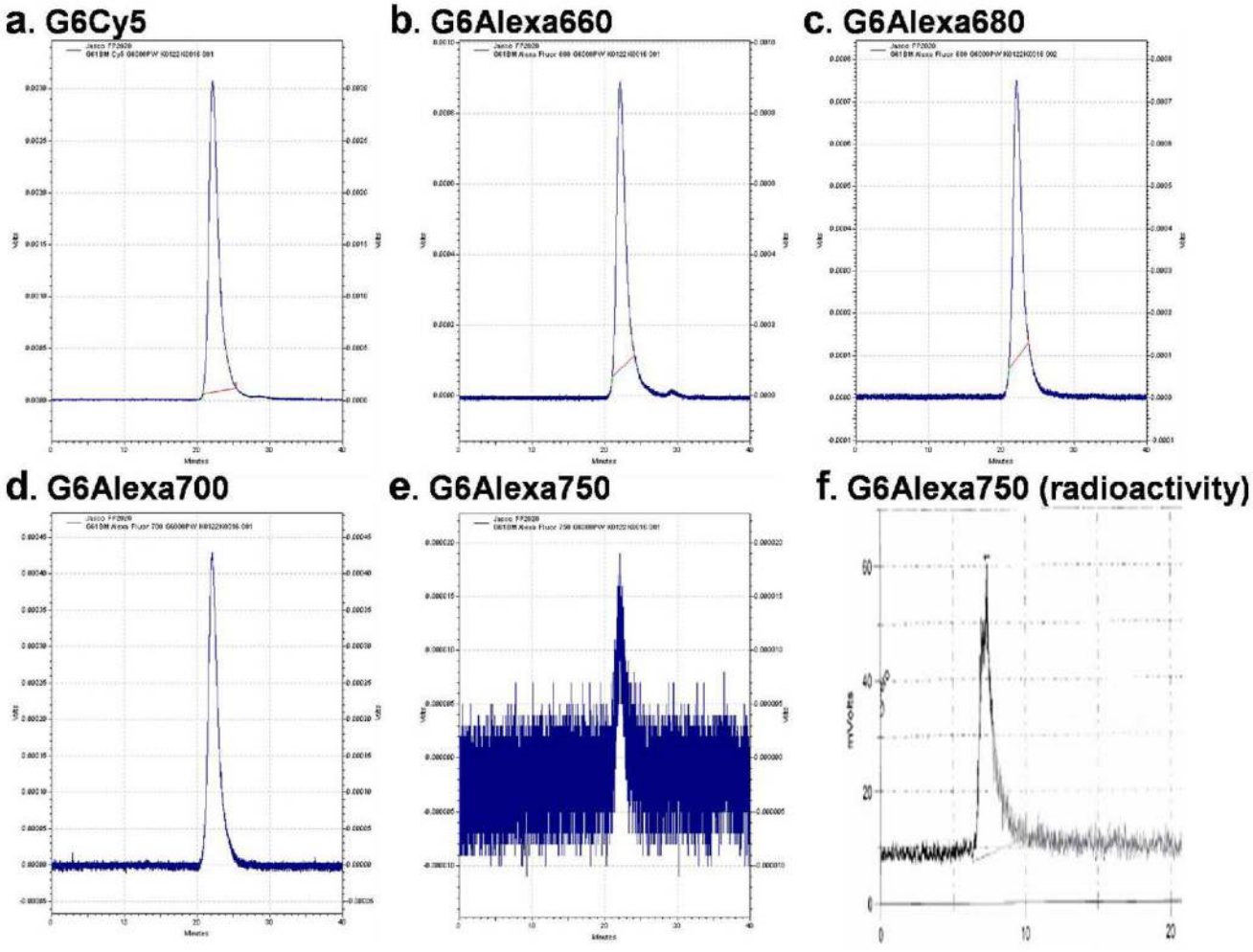

Figure 4. Fluorescent and radioactive purity of the final compound c was >98%

HPLC traces of all 5 final products **c: G6-(Bz-DTPA)$_{119}$-(NIR)$_4$-(Bz-DTPA-111In)$_1$** (NIR dyes, a: Cy5, b: Alexa660, c. Alexa680, d: Alexa700, e. Alexa750) obtained with a fluorescence detector are shown. All peak retention times of 5 compounds are 20.67 min on the size-exclusion HPLC using a TSK G6000PW column. Since the fluorescence detector was less sensitive for Alexa750 resulted in small peaks, another HPLC trace of **G6-(Bz-DTPA)$_{119}$-(Alexa750)$_4$-(Bz-DTPA-111In)$_1$** obtained with a radioactivity detector are shown. The peak retention time of this compound is 7.31 min on the size-exclusion HPLC using a TSK G3000PWxL column. The other 4 compounds showed identical radioactive HPLC traces and exactly the same retention time.

TABLE 1

Summary of Injection Pattern for *in vivo* 5-color Spectral Fluorescence Lymphatic Imaging.

Animal#	Rt. hand	Lt. hand	Rt. ear	Lt. ear	Median chin
1	Cy5	Alexa660	Alexa700	Alexa680	Alexa750
2	Alexa680	Alexa700	Alexa750	Cy5	Alexa660
3	Alexa750	Alexa680	Cy5	Alexa660	Alexa700
4	Alexa660	Alexa750	Alexa680	Alexa700	Cy5
5	Alexa700	Cy5	Alexa660	Alexa750	Alexa680
Dual-modal					
6	Cy5	Alexa660	Alexa700	Alexa680	Alexa750
7	Alexa750	Alexa700	Alexa660	Cy5	Alexa680
8	Alexa660	Alexa680	Alexa750	Alexa700	Cy5-